Bull Eng Geol Environ (2012) 71:359–366
DOI 10.1007/s10064-011-0386-3

ORIGINAL PAPER

Computational fluid dynamics modeling of post-liquefaction soil flow using the volume of fluid method

Yu Huang · Wuwei Mao · Hu Zheng · Guanghui Li

Received: 5 November 2010 / Accepted: 28 May 2011 / Published online: 29 June 2011

Abstract Flow deformation of post-liquefaction soil during an earthquake can cause serious damage to engineering structures. To overcome the limitations of conventional deformation analysis methods based on solid mechanics for extremely large systems, a computational fluid dynamics (CFD) method is proposed to numerically simulate the flow behavior of post-liquefaction soil. The liquefied soil is assumed to be a viscous fluid, and the volume of fluid (VOF) model is used for interface tracking in the numerical scheme. The results of a modeling test conducted on liquefaction-induced ground flow to verify the validity of the method showed good agreement, indicating the proposed method is capable of being used to reproduce the flow behavior of post-liquefaction soil.

Keywords Soil liquefaction · Flow failure · Earthquake · Computational fluid dynamics · Volume of fluid method

Résumé Les écoulements après liquéfaction de sols pendant un séisme peuvent causer de sérieux dommages aux ouvrages. Afin de surmonter les limitations des méthodes conventionnelles d'analyse des déformations basées sur la mécanique des solides appliquée à des grands systèmes, une méthode numérique de dynamique des fluides (CFD) est proposée pour simuler numériquement l'écoulement après liquéfaction du sol. Le sol liquéfié est supposé être un fluide visqueux et le modèle du volume de fluide (VOF) est utilisé pour suivre les interfaces dans le schéma numérique. Les résultats d'un test de modélisation, destiné à vérifier la validité de la méthode et réalisé à partir d'un écoulement de terrain consécutif à un processus de liquéfaction, ont permis de conclure que la méthode proposée peut être utilisée pour reproduire le comportement du sol après liquéfaction.

Mots clés Liquéfaction de sol · Ecoulement · Séisme · Dynamique des fluides · Modélisation · Méthode du volume de fluide

Y. Huang (✉)
Key Laboratory of Geotechnical and Underground Engineering of the Ministry of Education, Tongji University, Shanghai 200092, China
e-mail: yhuang@tongji.edu.cn

W. Mao · H. Zheng · G. Li
Department of Geotechnical Engineering, Tongji University, Shanghai 200092, China

G. Li
CCCC Third Harbor Consultants Co. Ltd, Shanghai 200032, China

Introduction

In recent years, liquefaction resulting from seismic events has become a major concern due to its impact on structures, buildings and other infrastructure during and after an earthquake. Almost all major earthquakes are accompanied by soil liquefaction, as evidenced by the 1976 Tangshan earthquake in China (Fu and Tatsuoka 1984), the 1989 Loma Prieta earthquake in the USA (Bartlett and Youd 1995), the 1995 Hyogo-ken-Nambu earthquake in Japan (Shibata et al. 1996), and the 2008 Wenchuan earthquake in China (Huang and Jiang 2010). Liquefaction-induced ground failure has become one of the leading causes of infrastructure damage during an earthquake. Under seismic loading, the rapid increase in pore water pressure quickly decreases the shear strength of the unconsolidated sediment, possibly triggering large shear deformation. As flow failure of the ground during an earthquake may be caused

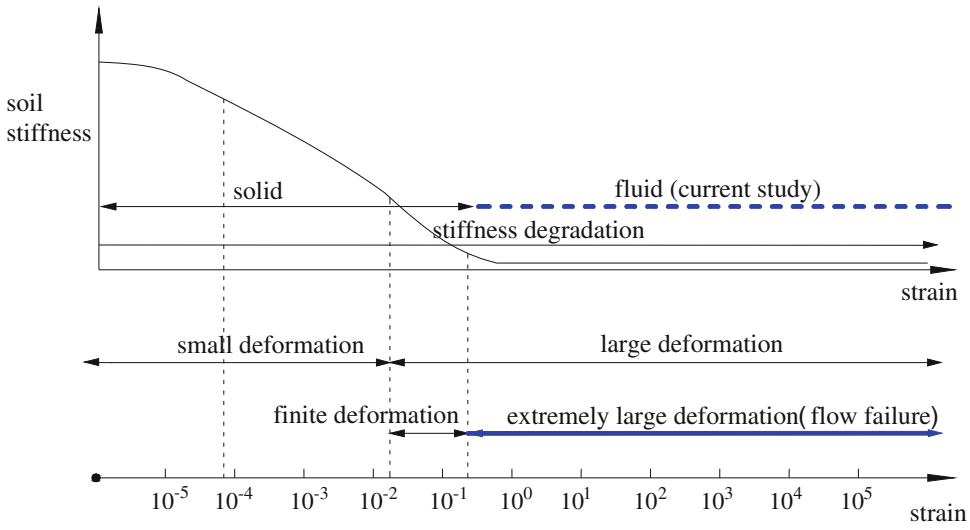

Fig. 1 The mechanical state of the liquefied soil under loading

by either the dynamic force due to the seismic acceleration or the static gravity force due to the topography of the ground (Tamate and Towhata 1999), flow deformation of post-liquefaction soil may continue under a gravitational load after seismic shaking ceases. In this case, the ground surface is prone to large-scale flow deformation regardless of whether it is flat or gently inclined. Uzuoak et al. (1998) suggests the shear strain may sometimes exceed 100%. This can develop into a regional seismic liquefaction event that can cause extensive damage. During the Tajik earthquake in 1989, the sliding mass traveled a distance of 2 km due to the liquefaction of the saturated soil, despite the fact that the ground surface was nearly flat (Ishihara 2009). More recently, during the 2003 Tokachi-oki earthquake in Japan, fluidized subsurface soil was expelled onto the surface and flowed about 1 km along a water channel (Kokusho 2009).

Liquefaction hazards are associated with substantial losses. Compared with the liquefaction itself, the damage resulting from the large scale deformation of the liquefied soil can be even more serious. Previous studies of soil liquefaction have mainly focused on influencing factors, initial conditions and liquefaction predictions, and only recently has attention turned to the importance of the large deformation associated with liquefaction. These studies generally use conventional solid mechanics-based methods and assume a relatively limited maximum shear (Yang and Elgamal 2002; Yoshimine et al. 2006). However, with liquefaction-induced ground flow, the shear strain of the soil may exceed 100% in the flow condition (Fig. 1), i.e, the state of the soils has been changed from solid to fluid.

In the past few years, a series of laboratory tests conducted by different researchers has shown that post-liquefaction soil behaves in a similar manner to a viscous fluid (Sasaki et al. 1992; Towhata et al. 1999; Hwang et al. 2006). Thus, due to the phase transition, it is difficult to apply solid mechanics based on small or finite deformation theory to the deformation properties of the post-liquefaction soil; a new analytical method is required.

Computational fluid dynamics (CFD) is a computer-based method which makes use of a discretization of the algebraic equations governing flow and their subsequent mathematical manipulation and solution (Versteeg and Malalasekera 1995). With the development of computer technology, numerical simulation methods have been rapidly developed, expediting the use of such applications as the CFD method to the study of liquefaction-induced flow deformation. In recent years, a few preliminary attempts have been made to promote the application of the CFD method to deformation problems related to liquefaction (e.g., Uzuoka et al. 1998; Hadush et al. 2001; Hwang et al.

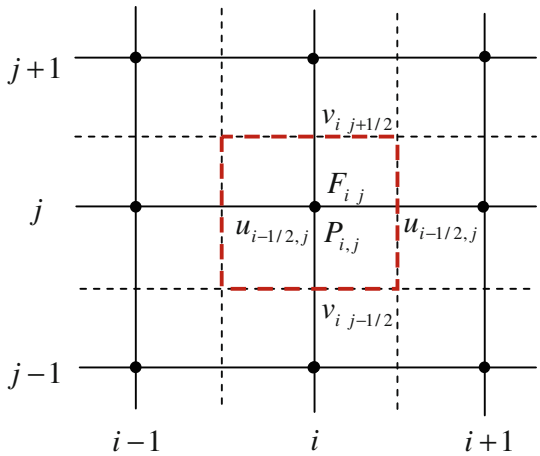

Fig. 2 Locations of variables in staggered grid

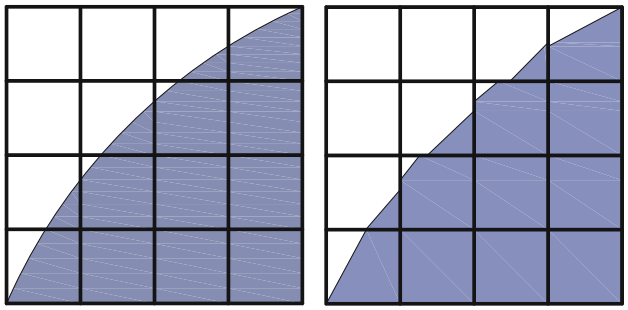

a actual interface shape **b** reconstructed interface shape

Fig. 3 Comparison of actual and reconstructed interface shapes represented by geometric reconstruction

2006). However, the research is very limited compared with that using solid mechanics and hence there is no generally accepted theory concerning its use in describing non-linear and deformation characteristics. In addition, little material is available concerning the study of large deformation flows induced by liquefaction.

The present study is a further development in the ongoing efforts to assess the flow features of post-liquefaction soils. In this paper, the post-liquefaction soil is assumed to be a viscous fluid, and a numerical model based on fluid dynamics is proposed for the flow behavior. The Pressure Implicit with Splitting of Operators (PISO) algorithm is used for solving the Navier–Stokes equations, and the volume of fluid (VOF) model is used to track interfaces in the numerical scheme. To verify the validity of the method, modeling of the liquefaction-induced soil flow was undertaken.

Numerical model description

The numerical modeling of ground flow involves the solution of the Navier–Stokes equations, which are based on the assumption of the conservation of mass and momentum, and the tracking of phase interface kinematics. The conservation of mass is described by the following equation:

$$\frac{\partial \rho}{\partial t} + \nabla(\rho \boldsymbol{u}) = 0, \tag{1}$$

and the conservation of momentum is described as:

$$\frac{\partial \rho \boldsymbol{u}}{\partial t} + \nabla(\rho \boldsymbol{u}\boldsymbol{u}) = \rho \boldsymbol{f}_v + \nabla \boldsymbol{T}. \tag{2}$$

In this paper the fluid is assumed to follow the generalized Newton's Law; the constitutive model can be described by the following equation:

$$\boldsymbol{T} = -p\boldsymbol{I} + 2\eta\left(\boldsymbol{S} - \frac{1}{3}\nabla \boldsymbol{u}\right). \tag{3}$$

Applying the constitutive model above to Eq. 2 results in the Navier–Stokes equation:

$$\frac{\partial \rho \boldsymbol{u}}{\partial t} + \nabla(\rho \boldsymbol{u}\boldsymbol{u}) = \rho \boldsymbol{f}_v - \nabla p + \nabla \boldsymbol{\tau} \tag{4}$$

where:

$$\nabla \boldsymbol{\tau} = \eta \Delta \boldsymbol{u} + \frac{1}{3}\eta \nabla(\nabla \boldsymbol{u}) \tag{5}$$

Note, in the equations above, the absence of sources of mass and momentum, where ρ is the fluid density, $\boldsymbol{S}$ is the strain rate tensor, $\boldsymbol{f}_v$ is the volume force, $\boldsymbol{u}$ is the velocity tensor, η is the viscosity, $\boldsymbol{T}$ is the stress tensor, p is the static pressure and $\boldsymbol{\tau}$ is the deviatoric stress tensor.

To solve the Navier–Stokes equations, the PISO algorithm (Issa 1986; Oliveira and Issa 2001) is used. This is a pressure–velocity calculation procedure based on a finite volume discretization on a staggered grid of the governing equations. The purpose of a staggered grid is to evaluate scalar variables, such as pressure and density, at ordinary nodal points, while velocities are defined at the cell faces between the nodes. The arrangement for a two-dimensional flow calculation is shown in Fig. 2. The PISO algorithm provides a higher degree of accuracy for pressure and velocity corrections than the SIMPLE algorithm (Barton 1998), which was used by Uzuoka et al. (1998) in the analysis of liquefaction-induced lateral spreading.

Due to the existence of a free surface with good mobility during the flow, a method for interface tracking can be used to describe the interface distribution and motion characteristics. In the past, a variety of methods, such as Level Set, Particle-In-Cell (PIC), Marker-and-Cell (MAC) and Volume of Fluid (VOF) have been developed for phase interface tracking (Oliveira and Issa 2001; Andrews et al. 1996; Tomé et al. 2006; Hirt and Nichols 1981). The VOF method, which was initially introduced by Hirt and Nichols (1981), is known for its capacity for interface tracking, including stratified flows, free-surface flows, filling, sloshing and so on. As there is a typical phase interface existing between the air and the liquefied soil, the VOF method was considered appropriate for the description of flow configurations in post-liquefaction soil. The most important feature of the VOF method is the introduction of the phase function $F(x, y, t)$ for the description of the interface. F represents the areal (two-dimensional) or volumetric (three-dimensional) fraction of a cell being occupied by a fluid in the computational domain. If $F = 1$, the cell is full of a fluid phase; if F = 0, the grid is full of another fluid phase; if $0 < F < 1$, the cell is intersected by the phase interface. The position of the interface is

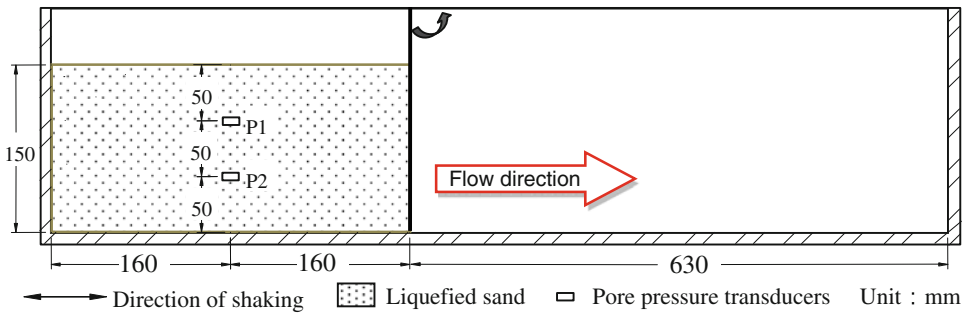

Fig. 4 Configuration of the model box equipped with transducers for liquefaction tests

Table 1 Parameters for the sand used in the model tests

e_{max}	e_{min}	D_{50} (mm)	D_{30} (mm)	D_{10} (mm)
0.96	0.60	0.24	0.19	0.16

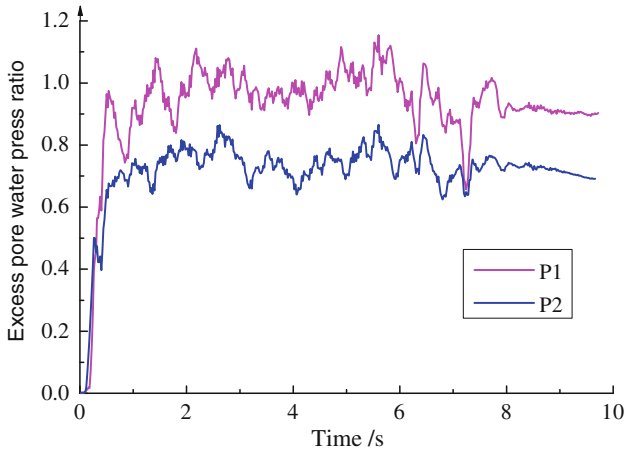

Fig. 5 Experimental time history of the excess pore water pressure ratio

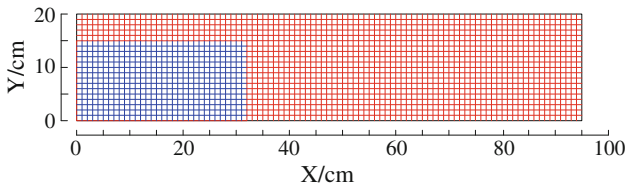

Fig. 6 Computational mesh

determined by the F values of the neighboring cells. For two immiscible flows, the conservation form of the transport equation is:

$$\frac{\partial F}{\partial t} + u\frac{\partial F}{\partial x} + v\frac{\partial F}{\partial y} = 0. \quad (6)$$

A detailed description of the VOF method is available in Hirt and Nichols (1981).

The Geometric Reconstruction scheme, which represents the interface between fluids using a piecewise linear approach, is applied to reconstruct the free surface between the liquefied

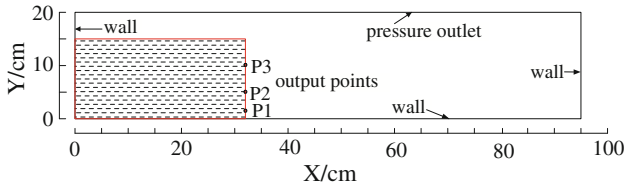

Fig. 7 Boundary conditions and position of output points

Table 2 Parameters used for the simulation of flow liquefaction

Density	1,600 (kg/m^3)
Viscosity	2,000 (Pa s)
Outlet pressure	1.013×10^5 (Pa)
Maximum iterations	30
Convergence criteria	1×10^{-3}
Total steps	1,000
Unit time step	0.005 (s)

soil and the air. As is shown in Fig. 3, the interface is described by a linear slope within each cell and the linear slope is used for the calculation of fluid flow through the cell faces. This approach is based on the work of Youngs (1982).

Applications and analysis

Model test description

Figure 4 shows the layout of the model box designed to reproduce and test the flow behavior of post-liquefaction soil. The soil container is made of transparent synthetic glass lined with an inner box. The external box is 950 mm long, 330 mm side and 350 mm high while the inner box is 320 mm long and 320 mm wide with a maximum height of 250 mm. The inclination of the model box may be changed if necessary. The properties of the sample sand used in the test are shown in Table 1. Liquefaction of the saturated soil sample in the inner box is generated by an electric motor which imparts a sinusoidal acceleration up to a maximum of 0.15 g at a frequency of 1 Hz. Excess pore water pressure is measured by pore pressure transducers installed at depths of 50 and 100 mm in

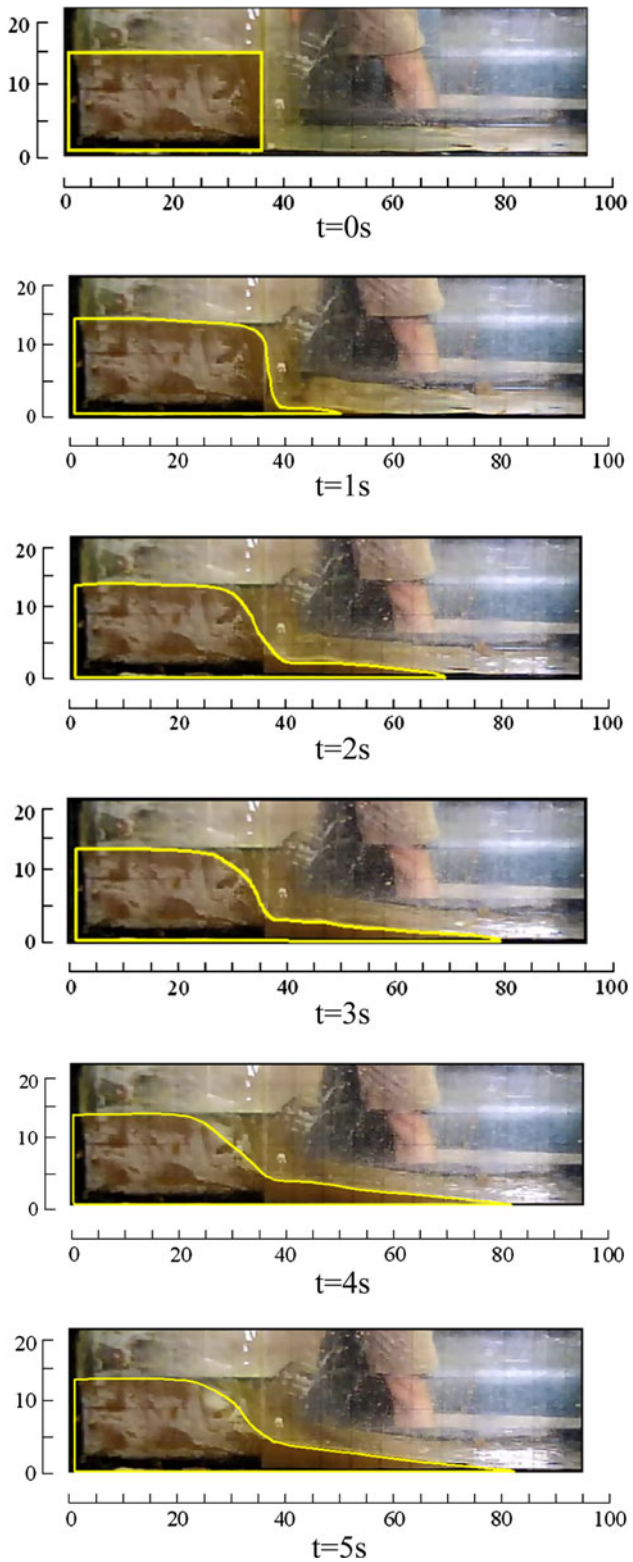

Fig. 8 Configuration of the model test

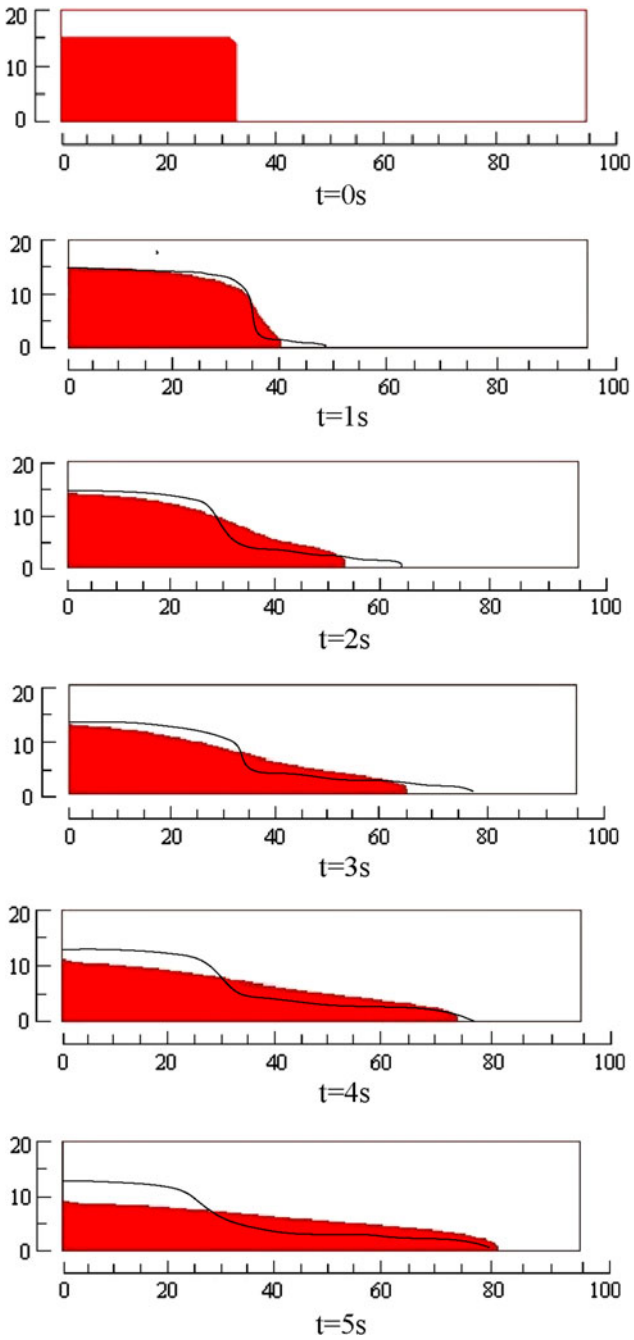

Fig. 9 Configuration comparison of model tests and simulation

the model. During the test, when the excess pore water pressure ratio (the ratio of excess pore water pressure to initial effective vertical stress) reaches 0.90 and remains stable (Fig. 5), the soil sample is considered to have reached the liquefaction state. The electric motor is then turned off, the baffle is quickly pulled out and the process of the post-liquefaction soil flow along the model box is recorded with a high-speed camera.

Model application

A finite volume method (FVM) with an Eulerian–Eulerian approach was used to study the air–liquid interactions. The

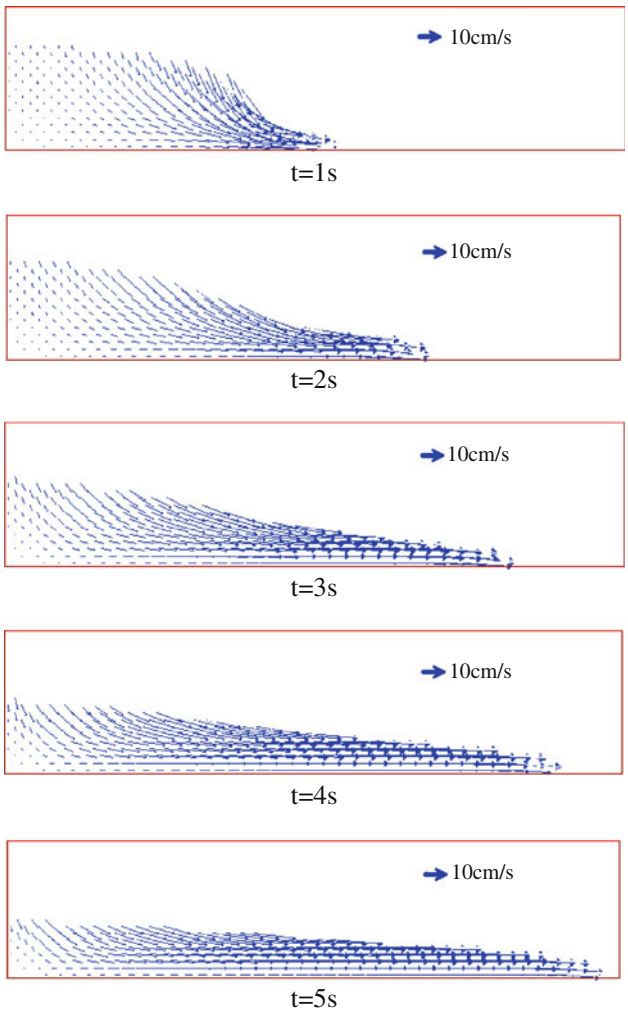

Fig. 10 Simulation results of velocity vectors

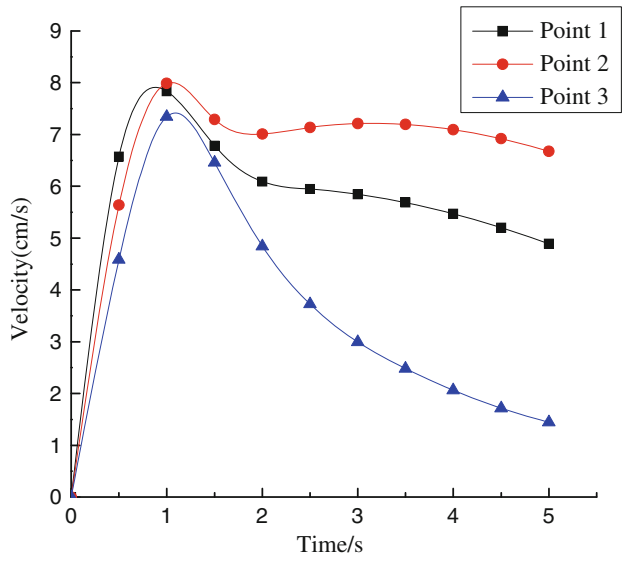

Fig. 11 Simulated time histories of velocities

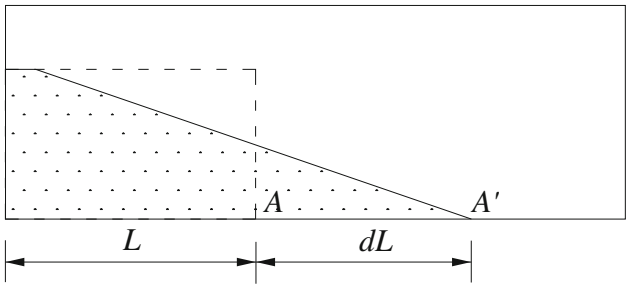

Fig. 12 Specified point selected for engineering strain calculation

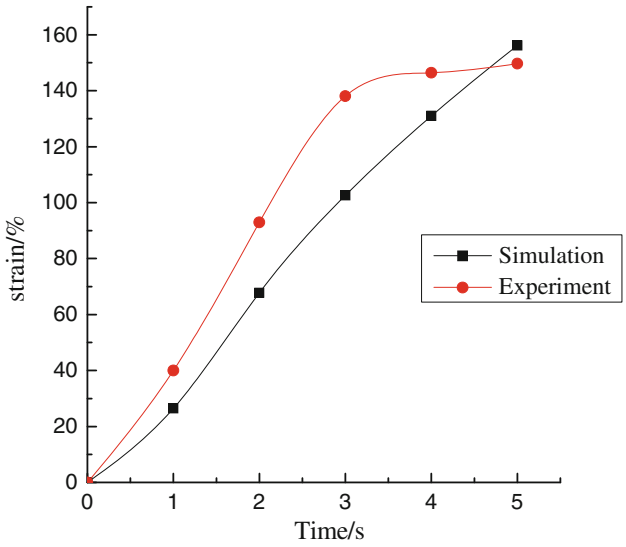

Fig. 13 Comparison of the engineering strain between model test and simulation results

phase-coupled PISO algorithm was used to couple the pressure and velocity. The diffusion phase of the control equation used the central difference method and the momentum equations used the first order upwind scheme.

The CFD code FLUENT 6.3, a well-known computer program for modeling fluid flow, was employed to verify the applicability of the proposed model (Fluent Inc 2006). Gambit 2.3.16 was used to generate the 2D geometries and their grids. As shown in Fig. 6, the length of the model box is 0.95 m and the height 0.20 m; by using a quadrilateral mesh, the overall number of nodes was 2,016 and the number of cells was 1,900. The left, right and bottom sides were set as WALL, which is used to bound fluid regions. The upper edge was set as PRESSURE-OUTLET to define a static pressure at the outlet boundary; here set to standard atmospheric pressure with a value of 1.013×10^5 Pa (Fig. 7). The model parameters used for the simulation of flow liquefaction are listed in Table 2.

Results and analysis

Figure 8 shows the configuration of the post-liquefaction sand flow obtained from the model test. The flow of the

liquefied sand gradually extended after the baffle was removed and lasted for 5 s. Figure 9 shows the flow configuration comparison of the model tests and simulation results for the post-liquefaction sand. It can be seen that, in general, the numerical approach reproduces the flow trend of the post-liquefaction sand and is in good agreement with the flow configuration. However, the simulated flow of sand was found to be a little faster than the flow recorded in the test. In the numerical simulation, the left side of the sand was observed to flow more substantially than in the model tests. Figure 10 shows the computed velocity vectors of the flow at a range of times from 1 to 5 s. It is clear that the velocity on the left side of the model had a very low magnitude. The vector directions indicate the flow orientation of the post-liquefaction sand.

Figure 11 shows the time histories of flow velocity at the selected output points depicted in Fig. 7. The flow of the post-liquefaction soil reaches its maximum velocity (from 8 to 9 cm/s) about 1 s after the instigation of flow. Thereafter, the flow begins to slow down. However, the degree of deceleration differs depending on the output point; the velocity at Point 3 decreased most quickly, followed by the velocities at Points 2 and 1. This is because Point 3 is closer to the free surface and is therefore more significantly affected by gravity, the main trigger of flow.

To evaluate laterally spreading features of the post-liquefaction sand flow, a simple calculation of engineering strain based on the one-dimensional movement of a specified point was carried out. Point A, in the lower right corner of the soil sample, was selected for this calculation (Fig. 12). Point A′ indicates the new location of Point A at different times during flow. L is the initial length of the soil sample, dL is the length increase in the flow direction; the engineering strain at Point A is defined as $\varepsilon = dL/L$. Figure 13 shows a comparison of engineering strain for the model tests and the numerical simulation results. It can be seen that in the first 3 s the simulated engineering strain was smaller than for the model test; however, this discrepancy decreases as the flow deformation progresses, with the values the same after 4 s of flow.

The strain-hardening behavior which occurs during flow is not considered here as the post-liquefaction soil is considered to be a viscous fluid. However, as evidenced by the model test, the excess pore water pressure dissipated rapidly and the liquefied soil recovered its strength, returning to the solid phase while still flowing. Thus, the simulation over-estimates the final flow deformation.

Conclusions

To overcome the limitations of traditional solid mechanics for the study of flow behavior in post-liquefaction soil, this paper presents a method based on fluid dynamics. 2D CFD simulations were conducted with a VOF model to predict the flow behavior of post-liquefaction soil, which is assumed to be a viscous fluid. The proposed model is capable of predicting flow liquefaction of soils in which the shear strain might exceed 100%.

A comparison of numerical and experimental results shows that the applied CFD method performs well, with the simulation showing a realistic lateral displacement and a velocity profile. The numerical approach reproduces the flow trend of the post-liquefaction sand and is in agreement with the model test flow configuration.

Acknowledgments This work was supported by the Key Laboratory of Engineering Geomechanics, Chinese Academy of Sciences (Grant No. 2008-04), the National Natural Science Foundation of China (Grant Nos. 41072202, 40802070 and 40841014), the Shanghai Municipal Education Commission and Shanghai Education Development Foundation (Shu Guang Project No. 08SG22), and the Kwang-Hua Fund for the College of Civil Engineering, Tongji University.

References

Andrews MJ, O'Rourke PJ (1996) The multiphase particle-in-cell (MPPIC) method for dense particulate flows. Int J Multiph Flow 22:379–402

Bartlett SF, Youd TL (1995) Empirical prediction of liquefaction-induced lateral spread. J Geotech Eng ASCE 121:316–329

Barton IE (1998) Comparison of SIMPLE- and PISO-type algorithms for transient flows. Int J Numer Methods Fluids 26:459–483

Fluent Inc (2006) Fluent users guide, Version 6.3. Lebanon, NH

Fu SC, Tatsuoka F (1984) Soil liquefaction during Haicheng and Tangshan earthquake in China; a review. Soils Found 24:11–29

Hadush S, Yashima A, Uzuoka R, Moriguchi S, Sawada K (2001) Liquefaction induced lateral spread analysis using the CIP method. Comput Geotech 28:549–574

Hirt CW, Nichols BD (1981) Volume of fluid (VOF) method for the dynamics of free boundaries. J Comput Phys 39:201–225

Huang Y, Jiang XM (2010) Field-observed phenomena of seismic liquefaction and subsidence during the 2008 Wenchuan earthquake in China. Nat Hazards 54:839–850

Hwang JI, Kim CY, Chung CK, Kim MM (2006) Viscous fluid characteristics of liquefied soils and behavior of piles subjected to flow of liquefied soils. Soil Dyn Earthq Eng 26:313–323

Ishihara (2009) Liquefaction-induced flow slide in the collapsible loess deposit in Tajik. Earthquake geotechnical case histories for performance-based design. Taylor & Francis Group, London, pp 431–448

Issa RI (1986) Solution of the implicitly discretized fluid flow equation by operator splitting. J Comput Phys 62:40–65

Oliveira PJ, Issa RI (2001) An improved PISO algorithm for the computation of buoyancy-driven flows. Numer Heat Trans Part B Fundam 40:473–493

Sasaki Y, Towhata I, Tokida K, Yamada K, Matumoto H, Tamari Y, Saya S (1992) Mechanism of permanent displacement of ground caused by seismic liquefaction. Soils Found 32:79–96

Shibata T, Oka F, Ozawa Y (1996) Characteristics of ground deformation due to liquefaction. Special issue on geotechnical aspects of the January 17, 1995 Hyogoken-Nambu earthquake. Soils and Foundations, pp 65–79

Tamate S, Towhata I (1999) Numerical simulation of ground flow caused by seismic liquefaction. Soil Dyn Earthq Eng 18:473–485

Tomé MF, Doricio JL, Castelo A, Cuminato JA, McKee S (2006) Solving viscoelastic free surface flows of a second-order fluid using a marker-and-cell approach. Int J Numer Methods Fluids 53:599–627

Towhata I, Vargas-Monge W, Orense RP, Yao M (1999) Shaking table tests on subgrade reaction of pipe embedded in sandy liquefied subsoil. Soil Dyn Earthq Eng 18:347–361

Tsukamoto Y, Ishihara K, Kokusho T (2009) Fluidisation and subsidence of gently sloped farming fields reclaimed with volcanic soils during 2003 Tokachi-oki earthquake in Japan. Earthquake Geotechnical Case Histories for Performance-Based Design. Taylor & Francis Group (London), 109–118

Uzuoka R, Yashima A, Kawakami T, Konrad JM (1998) Fluid dynamics based prediction of liquefaction induced lateral spreading. Comput Geotech 22:243–282

Versteeg HK, Malalasekera W (1995) An introduction to computational fluid dynamics. Pearson Education Limited, London

Yang ZH, Elgamal A (2002) Influence of permeability on liquefaction-induced shear deformation. J Eng Mech 128:720–729

Yoshimine M, Nishizaki H, Amano K, Hosono Y (2006) Flow deformation of liquefied sand under constant shear load and its application to analysis of flow slide of infinite slope. Soil Dyn Earthq Eng 26:253–264

Youngs DL (1982) Time-dependent multi-material flow with large fluid distortion. In: Morton KW, Baines MJ (eds) Numer Methods Fluid Dyn. Academic Press, New York